Doubling Reversible Capacities in Epitaxial $Li_4Ti_5O_{12}$ Thin Film Anodes for Microbatteries

Cunha, Daniel M.; Hendriks, Theodoor A.; Vasileiadis, Alexandros; Vos, Chris M.; Verhallen, Tomas; Singh, Deepak P.; Wagemaker, Marnix; Huijben, Mark

DOI
10.1021/acsaem.9b00217

Publication date
2019

Document Version
Final published version

Published in
ACS Applied Energy Materials

ACS APPLIED ENERGY MATERIALS

Article

Cite This: ACS Appl. Energy Mater. XXXX, XXX, XXX−XXX

www.acsaem.org

Doubling Reversible Capacities in Epitaxial $Li_4Ti_5O_{12}$ Thin Film Anodes for Microbatteries

Daniel M. Cunha,[†] Theodoor A. Hendriks,[†] Alexandros Vasileiadis,[‡] Chris M. Vos,[†] Tomas Verhallen,[‡] Deepak P. Singh,[†] Marnix Wagemaker,[‡] and Mark Huijben*[,†]

[†]MESA+ Institute for Nanotechnology, University of Twente, 7500 AE Enschede, The Netherlands

[‡]Faculty of Applied Sciences, Technical University Delft, 2629 JB Delft, The Netherlands

Supporting Information

ABSTRACT: Despite the lower gravimetric capacity, $Li_4Ti_5O_{12}$ is an important alternative to graphite anodes, owing to its excellent high temperature stability, high rate capability, and negligible volume change. Although surfaces with lithium compositions exceeding $Li_7Ti_5O_{12}$ were observed previously during the first charge−discharge cycles, no stable reversible capacities were achieved during prolonged cycling. Here, structural engineering has been applied to enhance the electrochemical performance of epitaxial $Li_4Ti_5O_{12}$ thin films as compared to polycrystalline samples. Variation in the crystal orientation of the $Li_4Ti_5O_{12}$ thin films led to distinct differences in surface morphology with pyramidal, rooftop, or flat nanostructures for respectively (100), (110), and (111) orientations. High discharge capacities of 280−310 mAh·g^{-1} were achieved due to significant surface contributions in lithium storage. The lithiation mechanism of bulk $Li_4Ti_5O_{12}$ thin films was analyzed by a phase-field model, which indicated the lithiation wave to be moving faster along the grain boundaries before moving inward to the bulk of the grains. The (100)-oriented $Li_4Ti_5O_{12}$ films exhibited the highest capacities, the best rate performance up to 30C, and good cyclability, demonstrating enhanced cycle life and doubling of reversible capacities in contrast to previous polycrystalline studies.

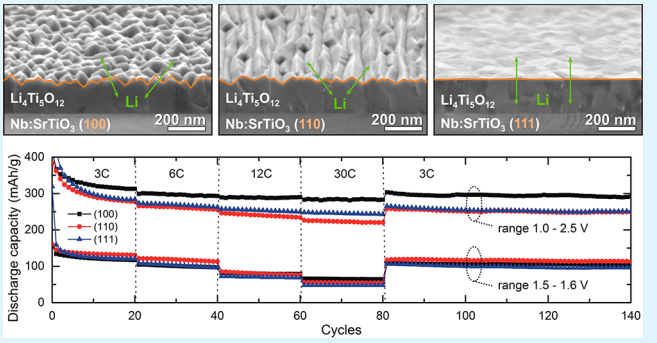

KEYWORDS: *battery anode, $Li_4Ti_5O_{12}$, epitaxial thin film, crystal orientation, surface capacity*

Lithium-ion batteries (LIBs) exhibit a unique combination of high energy and power densities, making it the technology of choice for portable electronics, power tools, and hybrid/full electric vehicles (EVs).[1,2] However, conventional state-of-the-art LIBs based on carbon anode materials, such as graphites, still do not fulfill the requirements for those high power applications due to poor safety characteristics. The spinel $Li_4Ti_5O_{12}$ (LTO) material has been extensively studied as an alternative to carbon anode materials in particular when cycle life and power density matters, because of its negligible volume change (0.2−0.3%), high rate capability, good safety characteristics, and high cycling stability.[3−6] LTO is a lithium intercalation compound exhibiting a theoretical capacity of 175 mAh·g^{-1} with a flat insertion/extraction voltage of approximately 1.55 V versus Li/Li$^+$, well above the potential for the formation of dendritic lithium and for the formation of a solid−electrolyte interphase (SEI) from the reduction of the organic electrolyte.[4] This advantage comes with compromise of a lower overall battery voltage decreasing energy density as compared to graphite anodes.[5,6] Although the native LTO exhibits low electronic conductivity (~10^{-8} to ~10^{-13} S·cm^{-1}) and low lithium-ion diffusion coefficient (~10^{-9} to ~10^{-16} cm^2·s^{-1}), considerable research on the morphological and surface optimization, doping, and nanostructuring has dramatically improved its capacity and rate capability.[3,4] Despite these advantageous properties, application of LTO is limited by a higher operating voltage and a lower capacity as compared to existing graphite anode.

Optimal performance of LTO relies on a fundamental understanding of the lithium diffusion kinetics and the underlying phase transformation mechanism. The defective spinel $Li_4Ti_5O_{12}$ can be indexed by the space group of *Fd*3*m* (*a* = 8.36 Å); see Figure 1a, in which tetrahedral 8a sites are occupied by Li$^+$ and octahedral 16d sites are occupied by Li$^+$ and Ti^{4+} randomly in a ratio of Li/Ti = 1/5, while the octahedral 32e sites are taken by O^{2-}. Therefore, $Li_4Ti_5O_{12}$ can be represented as $[Li_3]^{8a}[LiTi_5]^{16d}[O_{12}]^{32e}$. Lithiation leads to occupation of all of the octahedral 16c sites and emptying of the tetrahedral 8a sites to obtain the rock-salt-structured $Li_7Ti_5O_{12}$, which can be represented as $[Li_6]^{16c}[LiTi_5]^{16d}[O_{12}]^{32e}$; see Figure 1b. Although the lithiation process was for a long time understood as a two-phase reaction where the two end members coexist during

Received: January 30, 2019
Accepted: April 22, 2019
Published: April 22, 2019

DOI: 10.1021/acsaem.9b00217
ACS Appl. Energy Mater. XXXX, XXX, XXX−XXX

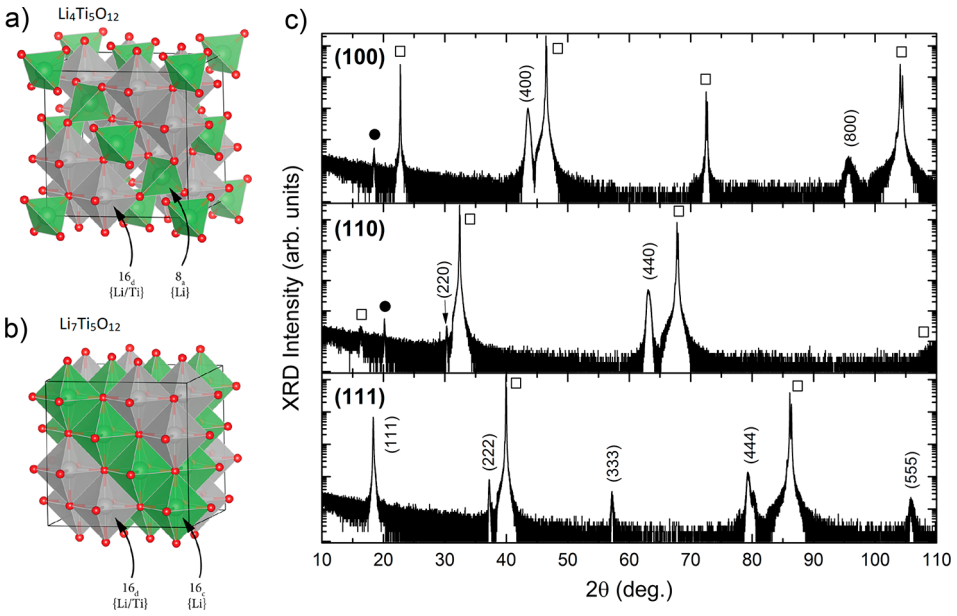

Figure 1. Schematics of the crystal structures of (a) spinel $Li_4Ti_5O_{12}$ and (b) rock-salt $Li_7Ti_5O_{12}$. (c) Out-of-plane XRD measurements of 220 nm $Li_4Ti_5O_{12}$ thin films on Nb-$SrTiO_3$ substrates with different crystal orientations: (100), (110), and (111). Peaks of the Nb-$SrTiO_3$ substrates are indicated by □, while minor contributions of β-Li_2TiO_3 are given by ●.

lithium insertion/extraction, recent studies have demonstrated that a solid solution exists with both $Li_4Ti_5O_{12}$ and $Li_7Ti_5O_{12}$ intimately mixed at nanometer length scales.[7−9] Furthermore, lithium compositions exceeding $Li_7Ti_5O_{12}$ have been observed during the first cycles experimentally[10−13] as well as theoretically,[14,15] indicating this to be a surface-related phenomenon.

The role of the surface on the storage properties of the spinel LTO anode was previously investigated by density functional theory (DFT) calculations to study the impact of the different crystal orientations at the anode surface ((100), (110), and (111)) on the voltage profiles.[15] It reveals that it is energetically more favorable to insert lithium into the (100) surfaces, leading to initially high voltages due to surface storage. The maximum observed bulk composition $Li_7Ti_5O_{12}$ can even be surpassed by lithium storage at the (111) surface facilitated by surface relaxation effects,[15] which explains the experimental higher capacities at voltages below the bulk voltage plateau.[10−13] It was predicted that increasing the relative amount of ⟨111⟩ facets would significantly increase the storage capacity, although the reversibility of this capacity could be limited by irreversible surface reactions at these high compositions. This surface environment with enhanced lithium content extended several nanometers into the anode material, leading to a distribution of voltages responsible for the curved voltage profiles in good agreement with experimental observations for epitaxial LTO films.[12,13]

However, most studies on epitaxial LTO thin films have focused on the structural properties of such oriented films,[16−19] which were deposited on insulating single crystalline substrates (e.g., $MgAl_2O_4$, α-Al_2O_3, and $SrTiO_3$), preventing the investigation of the electrochemical properties, whereas the only characterization of the electrochemical performance of epitaxial LTO thin films by Hirayama et al.[12,13,20] did demonstrate the cyclic voltammetry and charge−discharge curves of (110)- and (111)-oriented LTO films but did not explore the cyclability and rate performance of the specific crystal orientations. Highly controlled thin films make excellent model systems to study the lithiation mechanism in detail, to distinguish the surface capacities from bulk contributions, and to elucidate the possible limiting factors, including Li-ion diffusion, Li-ion transport, and electronic transport.

Here, we demonstrate the orientation-dependent intercalation kinetics for epitaxial $Li_4Ti_5O_{12}$ thin film anodes for which the electrochemical properties can be enhanced as compared to polycrystalline samples. Control of the specific orientation of the LTO thin film, and, therefore, the anode surface toward the adjacent electrolyte, was achieved by varying the crystal orientation of the single crystalline substrate ((100), (110), and (111)). All LTO films exhibit predominantly ⟨111⟩ crystal facets at their surfaces, which is the lowest energy state surface for this spinel structure. As a result the three types of LTO films exhibit dramatic differences in surface morphology with pyramidal, rooftop, or flat nanostructures for respectively (100), (110), and (111) orientations. All three crystal orientations showed high electrochemical performance with good cyclability without any significant capacity fading, as well as discharge capacities of 280−310 mAh·g^{-1} far above the theoretical capacity of the $Li_7Ti_5O_{12}$ composition. It is concluded from the layer thickness dependence that these high capacities are caused by significant surface contributions in lithium storage. When only the discharge capacity at the voltage plateaus (1.5−1.6 V range) is taken into account, a constant capacity of ∼120 mAh·g^{-1} is determined for all three crystal orientations in good agreement with the capacities determined from the layer thickness dependence. The lithiation mechanism of bulk $Li_4Ti_5O_{12}$ thin films was analyzed by a phase-field model, which indicated the lithiation wave to be moving faster along the grain boundaries before moving inward to the bulk of the grains. Because the (100)-oriented films exhibit an enhanced surface area for its pyramidal surface morphology, in contrast to the much flatter (110)- and (111)-oriented films, they show the highest capacities (1.0−2.5 V range) when cycling at various (dis)charging rates in the range of 3C−30C. These results show for the first time

DOI: 10.1021/acsaem.9b00217
ACS Appl. Energy Mater. XXXX, XXX, XXX−XXX

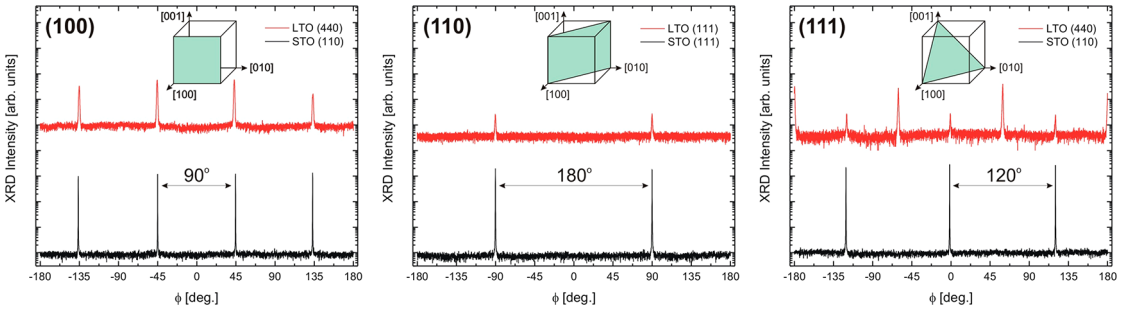

Figure 2. In-plane XRD measurements of 220 nm $Li_4Ti_5O_{12}$ thin films on Nb-$SrTiO_3$ substrates with different crystal orientations: (100), (110), and (111). Peaks of the $Li_4Ti_5O_{12}$ thin films and Nb-$SrTiO_3$ substrates are indicated respectively in red and black.

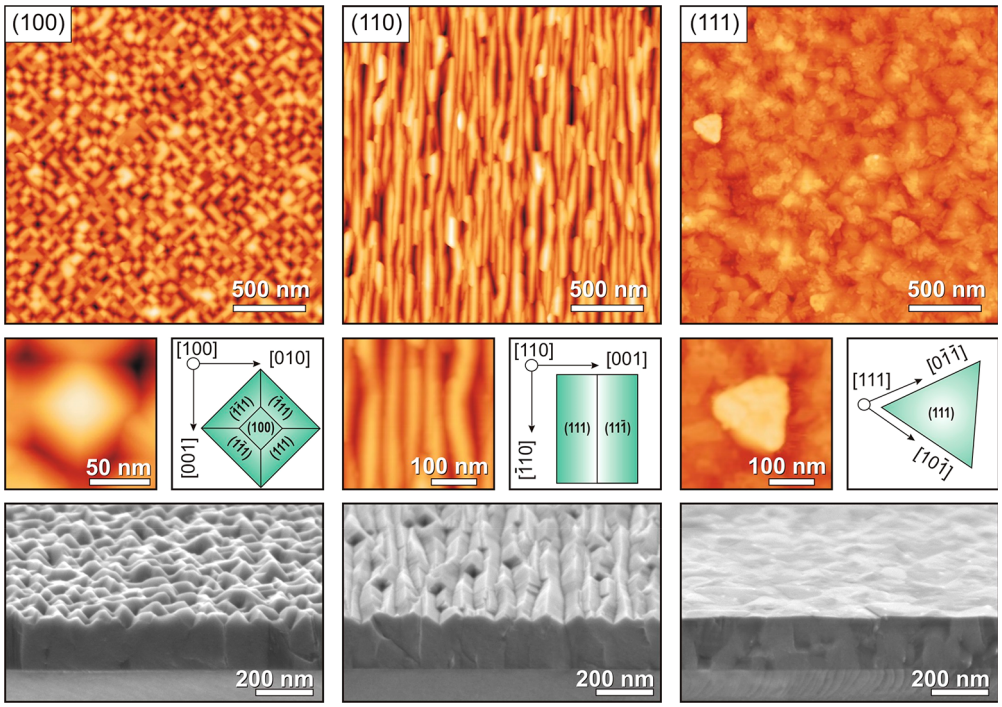

Figure 3. AFM (top) and SEM (bottom) analysis of the surface morphology of 220 nm $Li_4Ti_5O_{12}$ thin films on Nb-$SrTiO_3$ substrates with different crystal orientations: (100), (110), and (111). Schematics (middle) are shown of the expected crystal facets for the different surface morphologies.

experimentally that ⟨111⟩ crystal facets dramatically enhance the lithium storage of $Li_4Ti_5O_{12}$ thin film anodes due to significant surface contributions in lithium storage.

RESULTS AND DISCUSSION

In this study epitaxial engineering is applied as a tool to obtain improved control over the electrochemical properties of $Li_4Ti_5O_{12}$ thin films, which is unique for epitaxial thin films and cannot be obtained in single crystals or polycrystalline samples. Pulsed laser deposition (PLD) was used to grow $Li_4Ti_5O_{12}$ thin films on various single-crystal Nb-doped (0.5 wt %) $SrTiO_3$ (STO) substrates with different crystal orientations ((100), (110), and (111)). Details about the deposition conditions can be found in the Experimental Section and our previous study on epitaxial $LiMn_2O_4$ thin films.[21]

X-ray diffraction was used to investigate the structural quality of the LTO films, as shown in Figure 1c. The three types of LTO films exhibit coherent growth with the out-of-plane crystal orientation aligned to the orientation of the substrate. The LTO(111) films show the presence of a highly crystalline epitaxial layer, with a lattice parameter of ∼8.32 Å, without any impurity phase, in good agreement with previous study of LTO growth on STO(111) substrates.[12,20] This indicates the successful optimization of the PLD deposition process parameters (e.g., temperature, pressure, laser energy density, and target composition) to correct for any loss of volatile lithium during ablation, nucleation, or growth. However, the LTO films with (100) and (110) orientations still do show minor contributions of a secondary phase, although all three types of LTO films were grown during the same deposition procedure. The extra peaks at low diffraction angles cannot be ascribed to anatase or rutile TiO_2 as observed in previous studies[12,13] but suggest the presence of a small amount of monoclinic β-Li_2TiO_3 with respectively (002) or (110) orientation.[22] Although β -Li_2TiO_3 has also been investigated as anode material,[23] it will have a negligible effect on the electrochemical performance of the LTO thin films, as the anodic reduction and cathodic oxidation reactions in β -Li_2TiO_3 take place below ∼0.8 V.[23] This is far below the potential window in our measurements of 1.0−2.5 V.

Although large differences exist between the crystal structures of spinel LTO (a = 8.36 Å) and perovskite STO

DOI: 10.1021/acsaem.9b00217
ACS Appl. Energy Mater. XXXX, XXX, XXX−XXX

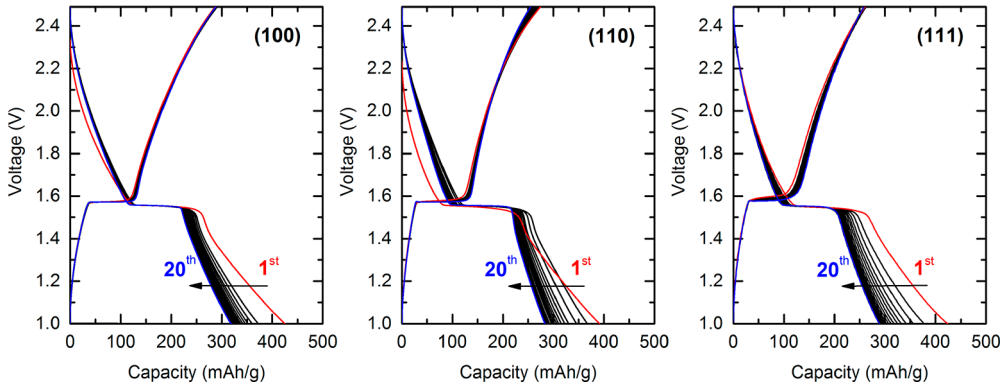

Figure 4. Charge−discharge analysis of the first 20 cycles on 220 nm $Li_4Ti_5O_{12}$ thin films on Nb-$SrTiO_3$ substrates with different crystal orientations ((100), (110), and (111)). During the measurements a current of 10 μA was used, which provided a (dis)charge rate of 3C.

(a = 3.90 Å), an epitaxial relation between the deposited LTO films and the underlying STO substrates is suggested by the alignment of their out-of-plane crystal orientations. Therefore, the in-plane crystal orientations of the LTO films were studied by XRD ϕ-scans along the LTO/STO directions of respectively (440)/(110), (111)/(111), and (440)/(110); see Figure 2. The separation of the STO peaks in the (100), (110), and (111) planes by respectively 90°, 180°, and 120° are consistent with the perovskite crystal structure, shown in the insets of Figure 2. For the LTO(100) and LTO(110) films the in-plane peaks are at the same angles as the substrate orientation indicating the in-plane alignment of the LTO layer to the STO structure. For the LTO(111) films the presence of two domains can be observed, in which part of the LTO layer is in-plane-aligned to the STO substrate but the majority is rotated 60° in-plane with respect to the substrate.

Detailed analysis of the surface morphology through atomic force microscopy (AFM) confirmed the preferred orientation of the LTO films; see Figure 3. Square-like structures with significant height differences (rms = ∼12.7 nm) can be observed at the surface of the LTO(100) film, which is in good agreement with previously observed octahedron spinel structures.[24,25] All four sides of such pyramidal spinel structures consist of ⟨111⟩ crystal facets with an occasional presence of a ⟨100⟩ crystal facet at the truncated top of the pyramid. These square-like structures confirm the 90° periodicity in the in-plane orientation as observed in XRD measurements; see Figure 2. Rooftop-like structures are formed at the surface of the LTO(110) films with a lower surface roughness (rms = ∼8.2 nm), caused by the anisotropic nature of the (110)-plane which favors diffusion of atoms along the [$\bar{1}$10]-direction as compared to the [001]-direction.[26] This results in elongated ⟨111⟩ crystal facets all aligned in the same direction in good agreement with the 180° periodicity observed in XRD results. Finally, triangle-like structures are formed at the surface of the LTO(111) films exhibiting a very low surface roughness (rms = ∼1.4 nm). The triangular shape corresponds to the (111)-plane in a cubic structure and matches the observed 120° periodicity in the XRD measurements. Furthermore, two different types of in-plane triangle orientations can be observed, which confirm the presence of two domain types, rotated 60° with respect to each other, as observed in XRD analysis. Therefore, surfaces exposing predominantly ⟨111⟩ crystal facets are present for all three types of LTO films with different out-of-plane orientations ((100), (110), and (111)), which confirms it as the lowest energy state surface. This is in good agreement with previous theoretical[15] and experimental[24] studies on LTO crystals, which demonstrated that oxygen-terminated (110) and (111) facets exhibit surface energies about half of a (100) facet due to the minimal loss of coordination to the subsurface TiO_6 octahedra, and much lower than lithium- or titanium-terminated surfaces.

The lithium intercalation characteristics were studied by galvanostatic charge−discharge analysis of electrochemical cells in which the LTO thin films were measured against lithium metal with a liquid electrolyte. Figure 4 shows charge−discharge curves from the first to the twentieth cycle for a constant current of 10 μA, corresponding to a (dis)charge rate of 3C, and cutoff voltages of 1.0 and 2.5 V. A clear voltage plateau could be observed around 1.55 V in good agreement with bulk LTO characteristics.[3,4] During the initial charge−discharge cycles of the LTO films, the charge capacity remains constant, while the discharge capacity is reducing toward a constant level. As a result, the calculated Coulombic efficiency is changing within this initial cycling toward ∼100%. However, when our LTO films are subsequently cycled at low rates of 3C within the voltage range between 1.0 and 2.5 V, the discharge capacity is always a little bit larger than the charge capacity, corresponding to a Coulombic efficiency of about 95%. This effect can also be observed in previous studies on epitaxial LTO thin films[12,13,20] as well as on polycrystalline LTO thin films,[27] but was never discussed specifically. Our LTO thin films do not exhibit an increase in internal resistance due to a growing SEI layer, but the experiments show a stable, reversible lithiation process. Therefore, it is suggested that the higher discharge capacity, as compared to the charge capacity, is due to a small increase in the SEI layer thickness which easily dissolves into the liquid electrolyte during subsequent charging. This process of SEI formation and dissolution at the LTO surface was previously demonstrated[28] and is much more pronounced in LTO thin films due to the limited volume of the samples. Further research is required to achieve detailed understanding on the contribution of the SEI layer for lithium storage in our LTO thin films systems.

All three crystal orientations showed high electrochemical performance with good cyclability, as well as very high discharge capacities far above the theoretical capacity of 175 mAh·g^{-1} for the $Li_7Ti_5O_{12}$ composition where all octahedral Li-positions are occupied. The total discharge capacity was the highest for the (100)-oriented LTO film, ∼313 mAh·g^{-1}, while the (110)- and (111)-oriented LTO films exhibit lower

DOI: 10.1021/acsaem.9b00217
ACS Appl. Energy Mater. XXXX, XXX, XXX−XXX

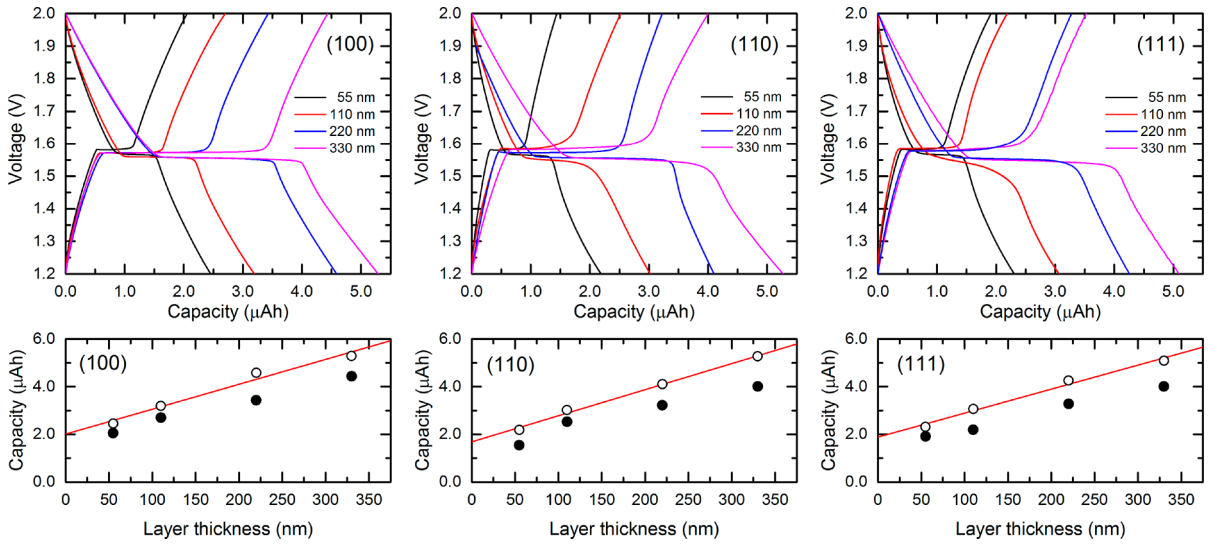

Figure 5. Layer thickness dependence of charge−discharge cycling (top) and total capacity (bottom) after charging (closed symbols) and after discharging (open symbols) of $Li_4Ti_5O_{12}$ thin films on Nb-$SrTiO_3$ substrates with different crystal orientations ((100), (110), and (111)). During the measurements a current was provided to result in a (dis)charge rate of 3C. Linear fits are shown for the thickness-dependent total discharge capacity.

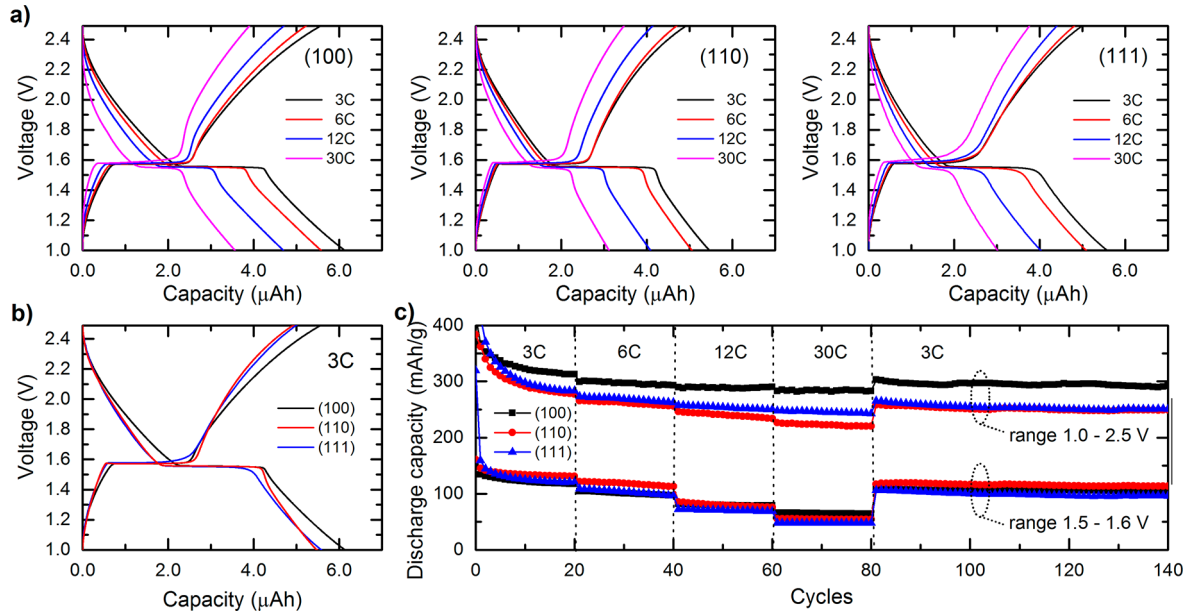

Figure 6. Charge−discharge rate dependence (a) of 220 nm $Li_4Ti_5O_{12}$ thin films on Nb-$SrTiO_3$ substrates with different crystal orientations ((100), (110), and (111)). During the measurements the current was varied between 10 and 100 μA, which led to a range of (dis)charge rates of 3C−30C. (b) Crystal orientation-dependent charge−discharge analysis at a rate of 3C. (c) Cycle life analysis of the discharge capacity at various rates determined over the full voltage range of 1.0−2.5 V or only the voltage plateau between 1.5 and 1.6 V. A potentiostatic period of 5 min is used to ensure complete charge or discharge before the next step.

discharge capacities of respectively ∼277 and ∼283 mAh·g^{-1}. The large surface area of the (100)-oriented LTO film, caused by pyramidal surface morphology, is suggested to cause the enhanced lithium storage as compared to the other crystal orientations. The crystal facets on all films are predominantly ⟨111⟩, which eliminates any possible effect from local variations in crystal facets. Surpassing the theoretical capacity for $Li_7Ti_5O_{12}$ composition is in good agreement with previous observations, although those theoretical models[14,15] and experimental studies on polycrystalline materials[10,11] required a voltage range from 2.5 V down to 0.01 V to realize lithiation up to $Li_{8.5}Ti_5O_{12}$ exhibiting capacities of ∼260 mAh·g^{-1}. Here, we achieve reversible high capacities of ∼280−310 mAh·g^{-1} for epitaxial films in the limited voltage range between 2.5 and 1.0 V, confirming the enhanced storage of lithium at the ⟨111⟩ facets.[15] Interestingly, our study shows such enhanced lithiation for all three film orientations ((100), (110), and (111)), all exhibiting ⟨111⟩ facets, in strong contrast to previous limitation to the (111) orientation.[12]

To distinguish the surface contribution from the bulk LTO layer dependent intercalation processes, variations in the electrochemical behavior were investigated for different LTO layer thicknesses. Figure 5 shows the charge−discharge curves for LTO film thicknesses in the range 55−330 nm together

DOI: 10.1021/acsaem.9b00217
ACS Appl. Energy Mater. XXXX, XXX, XXX−XXX

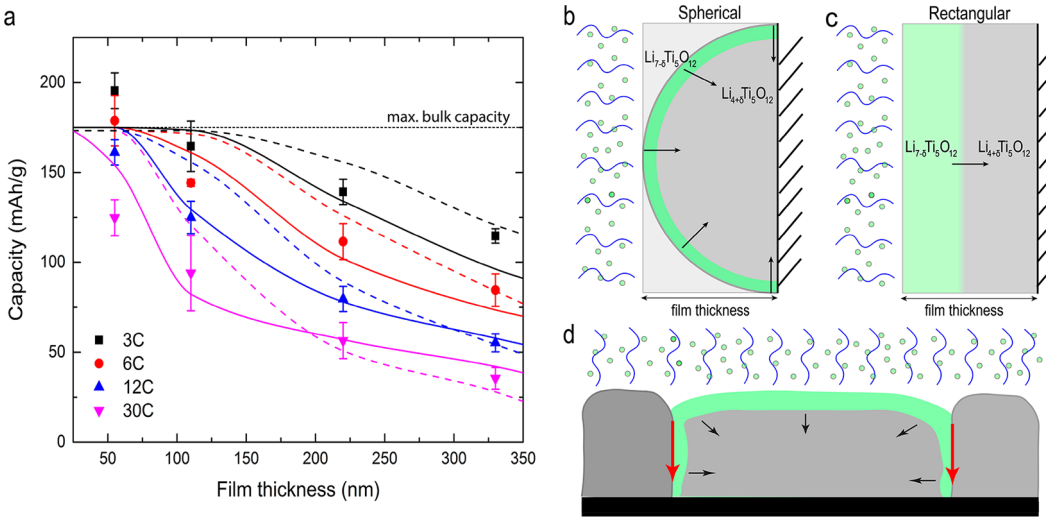

Figure 7. Lithiation mechanism in epitaxial $Li_4Ti_5O_{12}$ thin films on Nb-$SrTiO_3$ substrates. (a) Gravimetric discharge capacity dependence on film thickness for different C-rates, determined at the voltage plateau (1.5−1.6 V). Experimental results (symbols) and theoretical phase-field modeling for spherical approximation (dashed lines) and combined spherical and single-direction rectangular approximation (solid lines) are all shown. The two-phase lithiation model for (b) the spherical approximation, (c) single-direction rectangular approximation, and (d) the mixed approximation, combining spherical, and single-direction rectangular.

with the total capacity for each cell after charging or discharging. For the full thickness range and for all orientations the LTO films exhibit good electrochemical behavior with clear voltage plateaus as well as significant tails above and below those plateaus. The limited volume of the LTO layer in the thin films causes the surface contributions in the tails to be more pronounced as compared to bulk studies. It can be observed that for all three orientations the total capacities of the LTO films increase linearly with thickness, suggesting the presence of a volume-dependent capacity in combination with a constant surface capacity. The linear fits indicate similar volume-dependent discharge capacities of ∼120 mAh·g^{-1} for all orientations, while minimal variations can be observed for the offset on the capacity axes for the three orientations. These fits suggest the presence of a constant surface capacity of ∼8 μAh/cm^2 for all three orientations. This extra capacity cannot be completely stored within the LTO layer, as it would require an extra $Li_7Ti_5O_{12}$ layer with a thickness of about 130 nm. Therefore, the surface capacity can only partially be realized in a LTO layer with a higher lithiation level (i.e., $Li_9Ti_5O_{12}$). However, the SEI was recently suggested to act as an extra charge reservoir with a significant contribution to the reversible lithiation process.[29] The combination of both volume and surface contributions explains the measured large capacities in thin films (see Figure 4), and strongly points out the necessity to distinguish between them instead of calculating a full volumetric capacity as was done in previous studies.

The rate dependence of the discharge capacity for the LTO films with different crystal orientations is shown in more detail in Figure 6. After the initial 20 charge−discharge cycles with 3C (i.e., current of 10 μA), the films are consecutively cycled at various rates in the range 3C−30C (i.e., currents 10−100 μA) before finishing the sequence with the final 60 cycles with 3C. When our LTO films are cycled within the voltage range between 1.0 and 2.5 V, the Coulombic efficiencies are very close to 100% for a high (dis)charge rate of 30C and a few percent lower for a slow (dis)charge rate of 3C, as discussed before. High stability during substantial cycling is achieved for all LTO films, while the (100)-oriented film exhibits enhanced performance as compared to the other orientations. However, the capacity taken over the full voltage range of 1.0−2.5 V contains the surface capacity together with the volumetric capacity, and the surface capacity is significantly larger for the (100)-oriented LTO film due the large surface area of the pyramidal morphology. This difference in capacity can be explained by the variation in surface area between the differently oriented films, as the (100)-oriented films exhibit about 30% more surface area as compared to (110)- and (111)-oriented films, see Figure 3. When taking only the capacity at the voltage plateau (1.5−1.6 V) into account, the surface capacities do not contribute significantly and all three orientations show, at 3C, similar capacities of about 120 mAh·g^{-1}, in good agreement with the capacities determined from the layer thickness dependence. At the highest rate of 30C the LTO films still exhibit volumetric capacities of about 60 mAh·g^{-1}, in good agreement with values obtained for thick bulk LTO anodes.[30] The difference in measured capacities for the two voltage ranges suggest the presence of surface capacities of ∼15 μAh·cm^{-2} for (100)-oriented films and ∼12 μAh·cm^2 for (110)- and (111)-oriented films. Furthermore, the measured surface capacities remain highly reversible with good cyclability up to those high (dis)charge rates.

The lithiation mechanism of epitaxial LTO thin films was analyzed in detail by applying a phase-field model based on non-equilibrium electrochemical thermodynamics.[30] The model includes a thermodynamic description of the active material,[31−33] being able to capture phase separation in LTO electrodes and, coupled with a vacancy-based diffusion description in the solid, has been shown to correctly describe the material performance.[30] The model can only study Li-ion storage in the bulk and thus it is suitable to investigate the bulk capacities expected from the thin films, aiming to elucidate the possible limiting factors, including Li-ion diffusion, Li-ion transport, and electronic transport.

It is important to note that no thermodynamic or kinetic parameter was tuned to match the experimental results. All the parameters are identical to the ones reported in the prototypical case[26] and can be found in the Supporting

DOI: 10.1021/acsaem.9b00217
ACS Appl. Energy Mater. XXXX, XXX, XXX−XXX

Information. Regarding the geometrical features, the thin films are electrodes with practically zero porosity. In that sense, the surface of the thin film exposed to the electrolyte is expected to be completely wetted with no further Li-ion transport within the electrode due to the absence of pores. This hints that the diffusion coordinate within the solid particles, mimicking the grains of the thin film, needs to be in the order of magnitude of the film thickness. The absence of pores also indicates that the lithiation wave should propagate in a single direction (vertical to the film), from the liquid electrolyte toward the Nb-doped STO current collector. However, the existence of multiple interconnected grains is evident in the SEM images (Figure 3) and complicates the solid description. This is because the introduction of more grain boundaries is likely to result in more $Li_4Ti_5O_{12}/Li_7Ti_5O_{12}$ phase interfaces that have been shown to catalyze Li-ion diffusion.[9,34] This is also supported by electrodes build-up by large secondary particles consisting of smaller primary particles showing superior electrochemical performance.[4,35,36] Here, we investigate various particle shapes (spherical, cylindrical, and single-direction rectangular), which differ with regard to the volume fraction experienced as we move from the outside to the inside of the particle, and keep the Li-ion diffusion coordinate equal to the film thickness. Since all of the other parameters are experimentally determined, we can investigate which particle geometry captures the capacity trend as a function of current and film thickness best and, on the basis of the different volume fractions, draw conclusions regarding the effect of the interconnected grains.

The simulation results of the simple spherical approximation are plotted and fitted with a shape preserving interpolant, creating the trend lines depicted in Figure 7a including the experimental results for comparison. The experimental values resulted from averaging the bulk (1.5−1.6 V) capacities of all three oriented LTO films ((111), (100), and (110)) at the respective rates and thicknesses. The simulated trend lines match well with the decreasing capacity "staircase" observed experimentally. Excellent agreement is observed for the thicker LTO films (220 and 330 nm), while a larger capacity discrepancy is found for the thinner films where the simulated results converge faster to the theoretical maximum capacity. This is reasonable considering the fact that the ideal spherical approximation overestimates grain boundary diffusion (see Figure 7b and discussion in the Supporting Information) and the existence of larger errors in the measured capacity for thinner electrodes. However, the single-direction rectangular approximation, which initially may appear a realistic representation of the thin film batteries (see Figure 7c), predicts an extremely steep decrease in capacity with increasing thickness.

Our findings suggest that a mixed lithiation description, spherical and single-direction rectangular (see Figure 7d), appears the best description of the experimental results for the thinnest LTO films (55 and 110 nm); see Figure 7a. Thus, an exact multidimensional description of the grain geometry is required. This underlines the importance of understanding grain boundary diffusion and implies that the lithiation wave moves faster along the grain boundaries before moving inward to the bulk of the grain, creating radial-like lithiation conditions for the bulk LTO. In this way the role of grain boundaries[9,34] and the superior electrochemical behavior, encountered in literature among techniques utilizing large secondary particles,[4,35,36] is rationalized. We suggest that controlling the grain size is of great importance in order to tune the bulk capacity achievable for high C-rates in thin films.

Analysis of the possible rate limiting kinetic mechanisms and their contribution to the total overpotential was performed (see the Supporting Information). Li-ion transport through the electrolyte, electronic transport, and Li-ion transfer over the electrolyte−electrode contact all exhibit minimal contributions to the internal resistance and, hence, to the overpotentials that prevent utilizing the full capacity. The simulations confirm that the LTO thin films are limited completely by Li-ion diffusion in the solid phase, explaining the observed capacity loss with increasing current and thickness of material. Therefore, optimization of these batteries should focus on finding the optimum LTO thickness for the solid diffusion pathway or developing an intimate combination with a solid electrolyte with high ionic conductivity.

CONCLUSIONS

Improved control over the electrochemical properties of $Li_4Ti_5O_{12}$ thin films is enabled by structural engineering, which is unique for epitaxial thin films and cannot be obtained in single-crystal or polycrystalline samples. Dramatic differences in surface morphology with pyramidal, rooftop, or flat nanostructures were achieved by control in LTO thin films of the specific crystal orientation, respectively (100), (110), and (111). Surfaces exposing predominantly ⟨111⟩ crystal facets were present for all three types of LTO films, which confirmed it as the lowest energy state surface. All three crystal orientations showed high electrochemical performance with good cyclability without any significant capacity fading, as well as high discharge capacities of 280−310 $mAh{\cdot}g^{-1}$ exceeding the theoretical capacity of $Li_7Ti_5O_{12}$ (175 $mAh{\cdot}g^{-1}$). The layer thickness independence demonstrated that these high capacities are caused by large surface contributions in lithium storage, which cannot be fully explained by the presence of a $Li_9Ti_5O_{12}$ layer. Therefore, the contribution of the SEI layer to this reversible lithiation process requires further research. Furthermore, previous studies have used scan rate-dependent cyclic voltammetry to differentiate between diffusion-controlled intercalation and pseudocapacitive charge storage.[37,38] This method could provide some interesting insight into the observed surface capacity for our epitaxial LTO thin films, although its methodology is under strong debate as other studies have concluded it to be unsuitable for Nb-TiO_2 and $Li_4Ti_5O_{12}$ anode materials.[39]

The significance of our result is that in microbattery applications the advantages of LTO, such as high temperature stability, high rate capability, and negligible volume change, can be utilized without compromising capacity. The bulk capacity of the thin films is isolated when taking only the discharge capacity at the voltage plateaus (1.5−1.6 V range). This was confirmed with phase-field modeling simulations that matched the experimental decreasing capacity "staircase" with increasing thickness and current. The thin films are limited by Li-ion diffusion, and thus optimization should be pursued by tuning the film thickness. In addition, the computational investigation brings forward the importance of grain boundary diffusion. Fast lithiation along the grain boundaries is likely to create lithiation phase-fronts in the bulk of the grain that resemble more radial conditions rather than a strictly one-dimension lithiation front, vertical to the film. Thus, controlling the grain size and growth in such techniques is expected to affect the obtained bulk capacities. Since the

DOI: 10.1021/acsaem.9b00217
ACS Appl. Energy Mater. XXXX, XXX, XXX−XXX

(100)-oriented films exhibit an enhanced surface area for its pyramidal surface morphology, in contrast to the much flatter (110)- and (111)-oriented films, the (100)-oriented films provide the highest surface capacities when cycling at various (dis)charging rates in the range of 3−30C. These results show for the first time experimentally that ⟨111⟩ crystal facets dramatically enhance the lithium storage of $Li_4Ti_5O_{12}$ thin film anodes due to significant surface contributions in lithium storage.

EXPERIMENTAL SECTION

The $Li_4Ti_5O_{12}$ layers were grown by pulsed laser deposition (PLD) on conducting Nb-doped (0.5 wt %) single crystalline $SrTiO_3$ ((100), (110), and (111)) substrates from a sintered $Li_{4.8}Ti_5O_{12}$ (20 wt % excess Li_2O) target using a repetition rate of 5 Hz. During growth a temperature of 700 °C and an oxygen pressure of 0.2 mbar were used. Further details about the deposition conditions and substrate preparation can be found in a previous study on epitaxial $LiMn_2O_4$ thin films.[21] Thin films fabricated by pulsed laser deposition typically exhibit densities very close to theoretical values with negligible porosity. Therefore, the mass of the samples has been determined by using the theoretical density of LTO (3.51 g·cm^{-3}) together with the volume of the sample (thickness × 5 mm width × 5 mm length).

The crystal structure, surface morphology, and thickness of the thin films were investigated by X-ray diffraction (PANalytical X'Pert PRO diffractometer with Cu Kα radiation and 1/32 slit, in steps of 0.002° and 8.7 s/step), atomic force microscopy (Bruker ICON Dimension Microscope on tapping mode in air with Bruker TESPA-V2 cantilevers), and scanning electron microscopy (Zeiss Merlin HR-SEM), respectively.

For electrochemical characterization the LTO films were cycled galvanostatically against a lithium metal anode between 1.0 and 2.5 V with currents of 10, 20, 40, and 100 μA, corresponding to C-rates of approximately 3C, 6C, 12C, and 30C, respectively. Further details about the cell assembly and electrochemical measurements can be found in a previous study on epitaxial $LiMn_2O_4$ thin films.[21]

The LTO phase-field model is based on the modeling principles developed by Bazant and co-workers[31,32] and is described in detail, along with the parameters used, in the paper of Vasileiadis et al.[30] A thermodynamic description of the active material is achieved by including a regular solution model[31] that is able to distinguish between homogeneous lithiation and phase separation. The Gibbs free energy describing Li-ion insertion into LTO vacancies is approximated by the following equation:

$$g(\tilde{c}_s) = k_B T(\tilde{c}_s \ln(\tilde{c}_s)) + (1-\tilde{c}_s)\ln(1-\tilde{c}_s) + \Omega_a \tilde{c}_s(1-\tilde{c}_s) + \tilde{c}_s \mu_i^{\Theta} + \frac{1}{2}\frac{k}{c_{max}}|\nabla \tilde{c}_s|^2$$

where k_B is Boltzmann's constant, T the temperature in kelvin, $\tilde{c}_s$ the normalized concentration in the solid particles, Ω_a the enthalpy of mixing, μ_i^{Θ} the equilibrium potential versus Li/Li$^+$, and c_{max} the maximum concentration of Li. The variational differential of the Gibbs free energy with respect the Li concentration defines the diffusional chemical potential of Li ($\mu_{Li,LTO}$).

The most relevant property in this work is the Li-ion flux in the solid particles, which is proportional to the gradient of the diffusional chemical potential and can be expressed with a vacancy diffusion mechanism as follows, with D the diffusion of Li.

$$F = -\frac{D}{k_B T} c_s(1-\tilde{c}_s)\nabla \mu_{Li,LTO}$$

Analysis of the overpotentials limiting the battery was performed by simulating the thin films switching off one contribution to the overpotential at the time. This was possible by increasing the related property by several orders of magnitude. For example, switching off the overpotential contribution of Li-ion diffusion can be achieved by increasing the diffusivity of Li by a factor of 10^4. The overpotential contribution of Li-ion diffusion is then defined as the difference between the voltage profile of the thin film under the correct parameters and the voltage profile of the thin film under the same parameters with the only exception being the ultrahigh diffusion coefficient.

ASSOCIATED CONTENT

Supporting Information

The Supporting Information is available free of charge on the ACS Publications website at DOI: 10.1021/acsaem.9b00217.

Modeling of the grain boundary diffusion and analysis of the rate limiting kinetic mechanisms and their contributions to the total overpotential (PDF)

AUTHOR INFORMATION

Corresponding Author

*E-mail: m.huijben@utwente.nl.

ORCID

Marnix Wagemaker: 0000-0003-3851-1044

Mark Huijben: 0000-0001-8175-6958

Notes

The authors declare no competing financial interest.

ACKNOWLEDGMENTS

D.M.C., T.A.H., D.P.S., and M.H. acknowledge support by The Netherlands Organization for Scientific Research (NWO) under VIDI Grant No. 13456. A.V. acknowledges support by The Netherlands Organization for Scientific Research (NWO) under Grant No. 15785 and M.W. under VICI Grant No. 16122. T.W.V. acknowledges support from the Advanced Dutch Energy Materials (ADEM) program of the Dutch Ministry of Economic Affairs, Agriculture and Innovation.

REFERENCES

(1) Dahn, J.; Ehrlich, G. M., In *Linden's Handbook of Batteries*, 4th ed.; Reddy, T. B.; Linden, D., Eds.; McGraw Hill Professional, Access Engineering: New York, 2011.

(2) Nitta, N.; Wu, F.; Lee, J. T.; Yushin, G. Li-ion battery materials: present and future. *Mater. Today* **2015**, *18*, 252−264.

(3) Yi, T.-F.; Yang, S.-Y.; Xie, Y. Recent advances of $Li_4Ti_5O_{12}$ as a promising next generation anode material for high power lithium-ion batteries. *J. Mater. Chem. A* **2015**, *3*, 5750−5777.

(4) Zhao, B.; Ran, R.; Liu, M.; Shao, Z. A comprehensive review of $Li_4Ti_5O_{12}$-based electrodes for lithium-ion batteries: The latest advancements and future perspectives. *Mater. Sci. Eng., R* **2015**, *98*, 1−71.

(5) Yuan, T.; Tan, Z.; Ma, C.; Yang, J.; Ma, Z.-F.; Zheng, S. Challenges of Spinel $Li_4Ti_5O_{12}$ for Lithium-Ion Battery Industrial Applications. *Adv. Energy Mater.* **2017**, *7*, 1601625.

(6) Xu, G.; Han, P.; Dong, S.; Liu, H.; Cui, G.; Chen, L. $Li_4Ti_5O_{12}$-based energy conversion and storage systems: Status and prospects. *Coord. Chem. Rev.* **2017**, *343*, 139−184.

(7) Wagemaker, M.; Simon, D. R.; Kelder, E. M.; Schoonman, J.; Ringpfeil, C.; Haake, U.; Lützenkirchen-Hecht, D.; Frahm, R.; Mulder, F. M. A Kinetic Two-Phase and Equilibrium Solid Solution in Spinel $Li_{4+x}Ti_5O12$. *Adv. Mater.* **2006**, *18*, 3169−3173.

(8) Wagemaker, M.; van Eck, E. R. H.; Kentgens, A. P. M.; Mulder, F. M. Li-Ion Diffusion in the Equilibrium Nanomorphology of Spinel $Li_{4+x}Ti_5O_{12}$. *J. Phys. Chem. B* **2009**, *113*, 224−230.

(9) Ganapathy, S.; Vasileiadis, A.; Heringa, J. R.; Wagemaker, M. The Fine Line between a Two-Phase and Solid-Solution Phase Transformation and Highly Mobile Phase Interfaces in Spinel $Li_{4+x}Ti_5O_{12}$. *Adv. Energy Mater.* **2017**, *7*, 1601781.

DOI: 10.1021/acsaem.9b00217
ACS Appl. Energy Mater. XXXX, XXX, XXX−XXX

(10) Borghols, W. J. H.; Wagemaker, M.; Lafont, U.; Kelder, E. M.; Mulder, F. M. Size Effects in the $Li_{4+x}Ti_5O_{12}$ Spinel. *J. Am. Chem. Soc.* **2009**, *131*, 17786−17792.
(11) Ge, H.; Li, N.; Li, D.; Dai, C.; Wang, D. Study on the Theoretical Capacity of Spinel Lithium Titanate Induced by Low-Potential Intercalation. *J. Phys. Chem. C* **2009**, *113* (16), 6324−6326.
(12) Hirayama, M.; Kim, K.; Toujigamori, T.; Cho, W.; Kanno, R. Epitaxial growth and electrochemical properties of $Li_4Ti_5O_{12}$ thin-film lithium battery anodes. *Dalton Trans.* **2011**, *40*, 2882−2887.
(13) Kim, K.; Toujigamori, T.; Suzuki, K.; Taminato, S.; Tamura, K.; Mizuki, J.; Hirayama, M.; Kanno, R. Characterization of Nano-Sized Epitaxial $Li_4Ti_5O_{12}$(110) Film Electrode for Lithium Batteries. *Electrochemistry* **2012**, *80*, 800−803.
(14) Zhong, Z. Y.; Ouyang, C. Y.; Shi, S. Q.; Lei, M. S. Ab initio Studies on $Li_{4+x}Ti_5O_{12}$ Compounds as Anode Materials for Lithium-Ion Batteries. *ChemPhysChem* **2008**, *9*, 2104−2108.
(15) Ganapathy, S.; Wagemaker, M. Nanosize Storage Properties in Spinel $Li_4Ti_5O_{12}$ Explained by Anisotropic Surface Lithium Insertion. *ACS Nano* **2012**, *6*, 8702−8712.
(16) Kumatani, A.; Ohsawa, T.; Shimizu, R.; Takagi, Y.; Shiraki, S.; Hitosugi, T. *Appl. Phys. Lett.* **2012**, *101*, 123103.
(17) Kumatani, A.; Shiraki, S.; Takagi, Y.; Suzuki, T.; Ohsawa, T.; Gao, X.; Ikuhara, Y.; Hitosugi, T. Epitaxial growth of $Li_4Ti_5O_{12}$ thin films using RF magnetron sputtering. *Jpn. J. Appl. Phys.* **2014**, *53*, 058001.
(18) Li, N.; Katase, T.; Zhu, Y.; Matsumoto, T.; Umemura, T.; Ikuhara, Y.; Ohta, H. Solid−liquid phase epitaxial growth of $Li_4Ti_5O_{12}$ thin film. *Appl. Phys. Express* **2016**, *9*, 125501.
(19) Pagani, F.; Stilp, E.; Pfenninger, R.; Reyes, E. R.; Remhof, A.; Balogh-Michels, Z.; Neels, A.; Sastre-Pellicer, J.; Stiefel, M.; Döbeli, M.; Rossell, M. D.; Erni, R.; Rupp, J.L. M.; Battaglia, C. Epitaxial Thin Films as a Model System for Li-Ion Conductivity in $Li_4Ti_5O_{12}$. *ACS Appl. Mater. Interfaces* **2018**, *10*, 44494−44500.
(20) Hirayama, M.; Shibusawa, T.; Yamaguchi, R.; Kim, K.; Taminato, S.; Yamada, N. L.; Yonemura, M.; Suzuki, K.; Kanno, R. Neutron reflectometry analysis of $Li_4Ti_5O_{12}$/organic electrolyte interfaces: characterization of surface structure changes and lithium intercalation properties. *J. Mater. Res.* **2016**, *31*, 3142−3150.
(21) Hendriks, T. A.; Cunha, D. M.; Singh, D. P.; Huijben, M. Enhanced lithium transport by control of crystal orientation in spinel $LiMn_2O_4$ thin film cathodes. *ACS Appl. Energy Mater.* **2018**, *1*, 7046−7051.
(22) Kleykamp, H. Phase equilibria in the Li-Ti-O system and physical properties of Li_2TiO_3. *Fusion Eng. Des.* **2002**, *61−62*, 361−366.
(23) Lakshmi Narayana, A.; Dhananjaya, M.; Guru Prakash, N.; Hussain, O. M.; Julien, C. M. Nanocrystalline Li_2TiO_3 electrodes for supercapattery application. *Ionics* **2017**, *23*, 3419−3428.
(24) Wang, Q.; Guo, Q.; Hu, Y.; Li, B. High-quality spinel $LiCoTiO_4$ single crystals with co-exposed {111} and {110} facets: flux growth, formation mechanism, magnetic behavior and their application in photocatalysis. *CrystEngComm* **2016**, *18*, 6926−6933.
(25) Wang, F.; Wang, X.; Chang, Z.; Zhu, Y.; Fu, L.; Liu, X.; Wu, Y. Electrode materials with tailored facets for electrochemical energy storage. *Nanoscale Horiz.* **2016**, *1*, 272−289.
(26) Antczak, G.; Ehrlich, G. Jump processes in surface diffusion. *Surf. Sci. Rep.* **2007**, *62*, 39−61.
(27) Mosa, J.; Vélez, J. F.; Reinosa, J. J.; Aparicio, M.; Yamaguchi, A.; Tadanaga, K.; Tatsumisago, M. $Li_4Ti_5O_{12}$ thin-film electrodes by sol-gel for lithium-ion microbatteries. *J. Power Sources* **2013**, *244*, 482−487.
(28) Song, M.-S.; Kim, R.-H.; Baek, S.-W.; Lee, K.-S.; Park, K.; Benayad, A. Is $Li_4Ti_5O_{12}$ a solid-electrolyte-interphase-free electrode material in Li-ion batteries? Reactivity between the $Li_4Ti_5O_{12}$ electrode and electrolyte. *J. Mater. Chem. A* **2014**, *2*, 631−636.
(29) Rezvani, S. J.; Gunnella, R.; Witkowska, A.; Mueller, F.; Pasqualini, M.; Nobili, F.; Passerini, S.; Di Cicco, A. Is the Solid Electrolyte Interphase an Extra-Charge Reservoir in Li-Ion Batteries? *ACS Appl. Mater. Interfaces* **2017**, *9*, 4570−4576.
(30) Vasileiadis, A.; de Klerk, N. J. J.; Smith, R. B.; Ganapathy, S.; Harks, P.P.R.M.L.; Bazant, M. Z.; Wagemaker, M. Toward Optimal Performance and In-Depth Understanding of Spinel $Li_4Ti_5O_{12}$ Electrodes through Phase Field Modeling. *Adv. Funct. Mater.* **2018**, *28*, 1705992.
(31) Ferguson, T. R.; Bazant, M. Z. Nonequilibrium Thermodynamics of Porous Electrodes. *J. Electrochem. Soc.* **2012**, *159* (12), A1967−A1985.
(32) Bazant, M. Z. Theory of Chemical Kinetics and Charge Transfer based on Nonequilibrium Thermodynamics. *Acc. Chem. Res.* **2013**, *46* (5), 1144−1160.
(33) Smith, R. B.; Bazant, M. Z. Multiphase Porous Electrode Theory. *J. Electrochem. Soc.* **2017**, *164* (11), E3291−E3310.
(34) Wagemaker, M.; van Eck, E. R. H.; Kentgens, A. P. M.; Mulder, F. M. Li-Ion Diffusion in the Equilibrium Nanomorphology of Spinel $Li_{4+x}Ti_5O_{12}$. *J. Phys. Chem. B* **2009**, *113*, 224−230.
(35) Wang, C.; Wang, S. A.; He, Y. B.; Tang, L. K.; Han, C. P.; Yang, C.; Wagemaker, M.; Li, B. H.; Yang, Q. H.; Kim, J. K.; Kang, F. Y. Combining Fast Li-Ion Battery Cycling with Large Volumetric Energy Density: Grain Boundary Induced High Electronic and Ionic Conductivity in $Li_4Ti_5O_{12}$ Spheres of Densely Packed Nanocrystallites. *Chem. Mater.* **2015**, *27*, 5647−5656.
(36) Verde, M. G.; Baggetto, L.; Balke, N.; Veith, G. M.; Seo, J. K.; Wang, Z. Y.; Meng, Y. S. Elucidating the Phase Transformation of $Li_4Ti_5O_{12}$ Lithiation at the Nanoscale. *ACS Nano* **2016**, *10*, 4312−4321.
(37) Wang, J.; Polleux, J.; Lim, J.; Dunn, B. Pseudocapacitive Contributions to Electrochemical Energy Storage in TiO_2 (Anatase) Nanoparticles. *J. Phys. Chem. C* **2007**, *111*, 14925−14931.
(38) Brezesinski, T.; Wang, J.; Tolbert, S. H.; Dunn, B. Ordered mesoporous α-MoO_3 with iso-oriented nanocrystalline walls for thin-film pseudocapacitors. *Nat. Mater.* **2010**, *9*, 146−151.
(39) Opitz, M.; Yue, J.; Wallauer, J.; Smarsly, B.; Roling, B. Mechanisms of Charge Storage in Nanoparticulate TiO_2 and $Li_4Ti_5O_{12}$ Anodes: New Insights from Scan rate-dependent Cyclic Voltammetry. *Electrochim. Acta* **2015**, *168*, 125−132.

DOI: 10.1021/acsaem.9b00217
ACS Appl. Energy Mater. XXXX, XXX, XXX−XXX